Operation of a fiber-coupled laser-cooler down to cryogenic temperatures

Rémi Vicente, Giovanni Cittadino, Alberto Di Lieto, Mauro Tonelli, Arnaud Gardelein, Gilles Nogues

Research Article | Vol. 30, No. 8 / 11 Apr 2022 / Optics Express 12929

Optics EXPRESS

Operation of a fiber-coupled laser-cooler down to cryogenic temperatures

RÉMI VICENTE,[1,2,*] GIOVANNI CITTADINO,[3,4] ALBERTO DI LIETO,[3,4,5] MAURO TONELLI,[3,4,5] ARNAUD GARDELEIN,[1] AND GILLES NOGUES[2]

[1]Air Liquide Advanced Technologies, 2 rue de Clémencière BP 15, F-38360 Sassenage, France
[2]Institut Néel CNRS, Univ. Grenoble alpes, 25 avenue des Martyrs BP 166, F-38042 Grenoble cedex 9, France
[3]Dipartimento di Fisica, Universitá Di Pisa, Largo B. Pontecorvo 3, I-56127 Pisa, Italy
[4]Mega Materials srl, Largo B. Pontecorvo 3, I-56127 Pisa, Italy
[5]NEST Istituto di Nanoscienze-CNR, Piazza S. Silvestro 12, I-56127 Pisa, Italy
*remi.vicente@neel.cnrs.fr

Abstract: We report on the optical cooling of a 7.5%Yb:LiYF4 crystal down to 125 K in a multi-pass Herriott absorption cell, coupled via a single mode polarization maintaining optical fiber to the laser source. This configuration, never exploited before, is more practical for potential applications, in particular for space cryogenic setups. Moreover, the temperature reached is exactly the one needed in many setup embarked in small and medium satellites. We evaluate the heat load on the crystal at the minimum attainable temperature, which is comparable to state of the art systems.

1. Introduction

Since its first observation in 1995 [1], optical refrigeration of solids has made constant progresses over the last decades [2–4]. It relies on anti-Stokes fluorescence to extract heat from a solid down to cryogenic temperatures. Potential applications of this phenomenon include radiation-balanced lasers [5,6] and vibration-free cooling of devices in a temperature range which is not accessible to thermoelectric coolers. The latter is particularly appealing for space applications. For example, proper operation of focal plane IR detectors require temperatures below 150 K but their images can be blurred by micro-vibrations created by mechanical cryocoolers currently used in satellites. Morevover, in spite of a relatively low cooling efficiency which requires more power at satellites level, the compactness of an optical cryocooling head allows optical refrigeration to gain over pulsed-tube cooling in terms of volume and weight [7]. These figures become even better with recent improvements of cooling crystal efficiencies [8].

Beyond the stringent requirements in terms of power, footprint and weight, the practical implementation of optical cooling in space needs to separate the cooling head connected to the focal plane from the laser source used to excite the crystal. The most convenient link between these two elements is expected to be an optical fiber. It can easily find its path inside the satellite volume without disturbing the positioning of other instruments. Moreover, optical fibers are directly spliced to fiber laser amplifiers which could be used in order to provide the necessary laser power to pump the crystal. The requirements on the fiber link remain very stringent: it must convey tens of watts of laser power and maintain its linear polarization so as to optimize the absorption by the crystal. We report here on the first demonstration of a fiber-coupled lasercooling experiment where a LiYF4 crystal doped with 7.5% Yb^{3+} is pumped by a 1020 nm laser. For an absorbed power of 11.1 W, we are able to cool the crystal down to 125 K, thus reaching the cryogenic temperature range specifically needed in many setups on-board small satellites. Even

#448930 https://doi.org/10.1364/OE.448930
Journal © 2022 Received 18 Nov 2021; revised 25 Jan 2022; accepted 26 Jan 2022; published 4 Apr 2022

Optics EXPRESS

if the temperature reached in this experiment is higher than the minimum values reported in literature [9,10], our setup is capable of improvements, if needed.

2. Experimental setup

Our experimental setup is presented in Fig. 1. It is made of two parts linked by a single mode large mode area polarization maintaining fiber (Nufern PLMA-GDF-20-250-09 PM, core diameter 20 μm, $N_A = 0.09$). In the first part, the output of a 50 W – cw single-mode linearly polarized fiber laser (IPG Photonics PS-YLR-50-1020-LP) is coupled into the link fiber. The 1020 nm laser beam at the output of the laser collimator has a 5 mm diameter. It is first protected by an optical isolator followed by a variable reflective neutral density filter for tuning of its power and a shutter for protection of the experiment. A high power $\lambda/2$ waveplate aligns the laser polarization with the fiber optical axes. A $f = 60$ mm air-spaced achromatic doublet on a fiber launch system focuses the beam into the fiber which is held by a chuck. We measure a coupling efficiency of 95 % and a linear polarization degree at the output of the fiber higher than 98 %. We note that the fiber we use is the one which is used at the output of the laser. Hence the latter could then be directly sent to the second part of the experiment with no coupling loss. The purpose of this first part of the experiment is protection of the laser and easy replacement of the fiber. Moreover it allows to couple via a additional mirror an ancillary tunable Ti:Sapphire laser into the fiber for spectroscopy of the crystal.

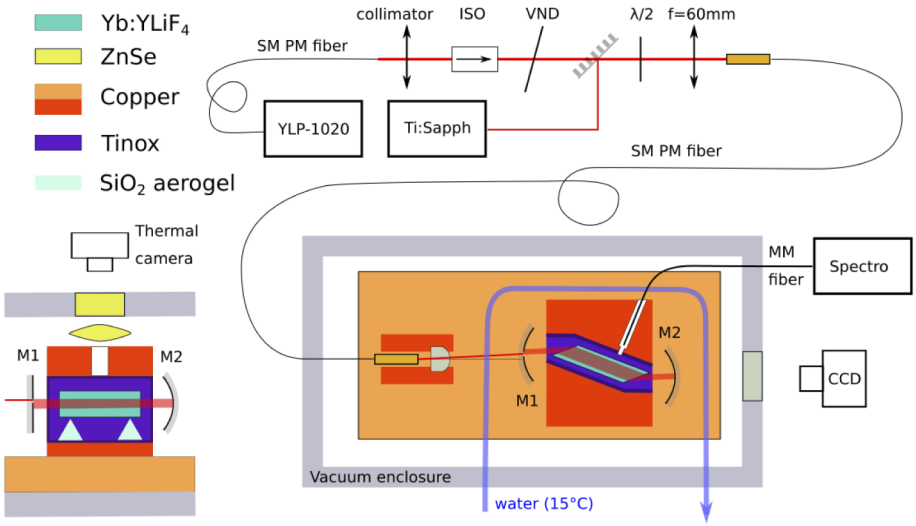

Fig. 1. Scheme of the experimental setup. ISO: optical Faraday isolator; VND: variable neutral density filter; SM PM: single mode polarization maintaining fiber; MM: multimode fiber; YLP-1020: 50 W – cw 1020 nm fiber laser.

The second part of the experiment corresponds to the cooling device. It is in a vacuum enclosure in order to reproduce space conditions and to reduce the convective heat load on the cooling crystal. The fiber enters the enclosure through a feedthrough. It is collimated by a homemade collimator made of a $f = 4.5$ mm aspheric lens (Thorlabs 354350-B) in a copper housing. Before operation of the experiment, the fiber is held by a fiber chuck whose position within the collimator is controlled with a three-axis translation stage. The chuck can also be rotated so as to change the polarization direction at the output. On an external alignment bench we control the fiber output in order to obtain a laser beam waist 30 mm behind the collimator (waist diameter 50 μm) and an horizontal polarization. We check that the laser makes a 0.8°

Optics EXPRESS

angle with the collimator optical axis in the horizontal plane. When the chuck is properly aligned it is glued to the collimator housing before being detached from the positioning stage. The collimator is then mounted on a XY translation stage in the experiment to couple the laser beam to an astigmatic Herriott multipass cavity. The latter is designed to maximize its interaction path with the cooling crystal [11,12]. The cavity is made of a $R_1 = 200$ mm cylindrical mirror M1, the cooling crystal (dimensions $2.5 \times 2.5 \times 9.5$ mm), whose entrance faces are cut at Brewster angle with respect to the laser polarization, and a $R_2 = 200$ mm spherical mirror M2. The distance between M1/M2 and the crystal is approximately 10 mm. The monocrystal is oriented and cut so that its c-axis is parallel to the laser polarization in order to maximize its absorption cross-section. Both mirrors are HR coated at 1020 nm. Moreover M1 coating has a $D = 90\,\mu$m hole with no-coating in order to let the laser beam enter the cavity. A CMOS camera observes the cavity spots behind mirror M2 in order to align the multipass cavity. Before placing the cooling crystal inside the cavity, a mock-up fused silica crystal with no absorption is used in the Herriott cell. After alignment, the reflection pattern on mirror M2 reproduces well the results of Ref. [12]. It allows more than 25 round-trips in the Herriott cell and hence for an absorption of the intracavity laser radiation larger than 99 % for temperature down to 130 K (single path absorption 8.8 %).

In order to reduce the thermal load on the cooling crystal, the latter is mounted on 2 mm-high silica aerogel pads (Ref Airloy X56) in order to limit the conduction losses. The vacuum enclosure is pumped down to 510−6 hPa to limit convection losses. And the crystal is surrounded by a Cu clamshell whose surface is covered by low-emissivity Tinox layer in order to limit thermal radiation losses. Thermal management of all systems not thermally connected to the crystal is achieved by a water circuit ($T_0 = 15\,^\circ$C) that flows through all Cu parts. The temperatures of the base, the clamshell cover and the collimator translation stage are are measured by Pt 100 Ω resistors.

3. Thermometers calibration

The crystal temperature is measured by two contact-free methods whose performances are discussed in the following.

3.1. Thermal camera imaging

First the crystal thermal radiation is imaged through a 3 mm hole in the clamshell onto a radiometric thermal camera (FLIR Lepton 3.5) outside the vacumm chamber. The collection lens and the vacuum window are made of ZnSe in order to transmit infra-red thermal radiation. The camera has a shutter that is closed during an internal automatic calibration process. We observe that the measured temperature readings from the camera are strongly perturbed for about 90 s after this process (the camera chipset temperature varies also during this period). In order to mitigate this effect, we have mounted the camera on a stage which is cooled down by the water flow, and all temperature measurements performed after the calibration process are discarded.

In order to properly account for the emissivity of YLF ϵ and the limited transmission of the imaging optics t we have observed a small piece of polished YLF in a He-flow cryostat (temperature T_c ranging from 120 to 300 K) with the same optical system. In order to assess the contribution of the emissivity we measure at the same time the temperature of a small piece of Aktar spectral black coating ($\epsilon = 0.98$) next to the crystal. We observe that, for temperatures above 240 K, the camera output varies linearly with crystal temperature. However for lower temperatures the thermal radiation impinging on the chip generates a signal which is no longer larger than the camera internal noise. Hence its reading deviates from the linear dependency. Below 160 K, the camera readings hold to an apparent temperature of 220 K and can no longer provide an information about the crystal temperature. For the 160 – 300 K range, we correct the camera temperature T_m in order to estimate the crystal temperature T_c with a calibration curve obtained by fitting the acquired data with a 3rd order polynomial.

Optics EXPRESS

3.2. Differential luminescence thermometry

Differential luminescence thermometry (DLT) is used for temperatures T below 160 K. A multimode optical fiber (Thorlabs MV42L05, NA = 0.22) collects the fluorescent light emitted by the crystal through a 0.8 mm hole in the clamshell. The light at the output of the fiber passes through a $\lambda = 1000$ nm short pass filter in order the remove the scattered laser light, and is focused back at the entrance of a Ocean's optics HR4000 spectrometer. We record the spectrum $S(\lambda, T)$ between $\lambda_1 = 900$ nm and $\lambda_2 = 1000$ nm and compute the normalized differential signal:

$$\Delta S(\lambda, T) = \frac{S(\lambda, T)}{\int_{\lambda_1}^{\lambda_2} S(\lambda, T) d\lambda} - \frac{S(\lambda, T_0)}{\int_{\lambda_1}^{\lambda_2} S(\lambda, T_0) d\lambda}, \tag{1}$$

where T_0 is a reference temperature. The normalisation of the signal ensures that the spectrum does not depend on the excitation power. The DLT signal is a measure of the spectral distance between T and T_0:

$$DLT(T, T_0) = \int_{\lambda_1}^{\lambda_2} |\Delta S(\lambda, T)| d\lambda \tag{2}$$

In usual DLT methods [13], the DLT signal is calibrated by recording fluorescence spectra in a separate cryostat at known temperatures, preferably in similar conditions as final observation conditions, i.e. with the same pump beam position inside the crystal and the same fluorescence collection system. The calibration function, which relates the DLT signal to the crystal's temperature can then be found. While suited for single pass experiments or small crystals, the "traditional" DLT method can never perfectly account for fluorescence re-absorption effects, and is not suitable for use with crystals in the astigmatic Herriott multipass cavity. Indeed, each passage of the laser in the multipass cavity contributes to the DLT signal, but the fluorescence spectrum for each path is different because of re-absorption. Hence it is not possible to use a DLT calibrated with spectra recorded in our ancillary cryostat which provides single path absorption. Additionally, the slightest variation in the multipass cavity alignment causes a change in the number of round-trips and their position inside the crystal. This translates in turn to a small variation of the perceived fluorescence spectral shape, sufficient to induce offsets from an external calibration function.

Here, we are using a variation of the DLT method, where the DLT signal is calibrated *in situ* in the experiment using the thermal camera as a reference thermometer above 160 K. The thermal camera combined with an extrapolated DLT calibration function below 160 K allows to be freed from fluorescence re-absorption issues when working with the multipass cavity. This technique, previously demonstrated before is described in Ref. [14]. It was shown to be accurate in predicting cooling crystals temperature variations, even with a difference of ΔT = 100 K between the lowest the thermal camera reading and the actual crystal temperature.

For each cooling run, the DLT signal is recorded together with the calibrated thermal camera measurements T_c. For every camera measurement, we evaluate the DLT by interpolating its value from the spectra taken just before and after the thermal image timestamp. We set $T_0 = T_c(t = 0)$. During the experiment of Fig. 2, we have set 4 different laser powers and checked that both thermal camera images and DLT are not affected by its variations. All DLT measurements versus T_c are fitted by a second order polynomial function in the 160 – 300 K range. The fit function is thereafter used for calculating the crystal temperature from the spectroscopic data (red cross in Fig. 2). Using that second order calibration function, the agreement between camera and spectroscopic measurements above 160 K is excellent. For temperatures under 160 K, we extrapolate the DLT calibration function.

Optics EXPRESS

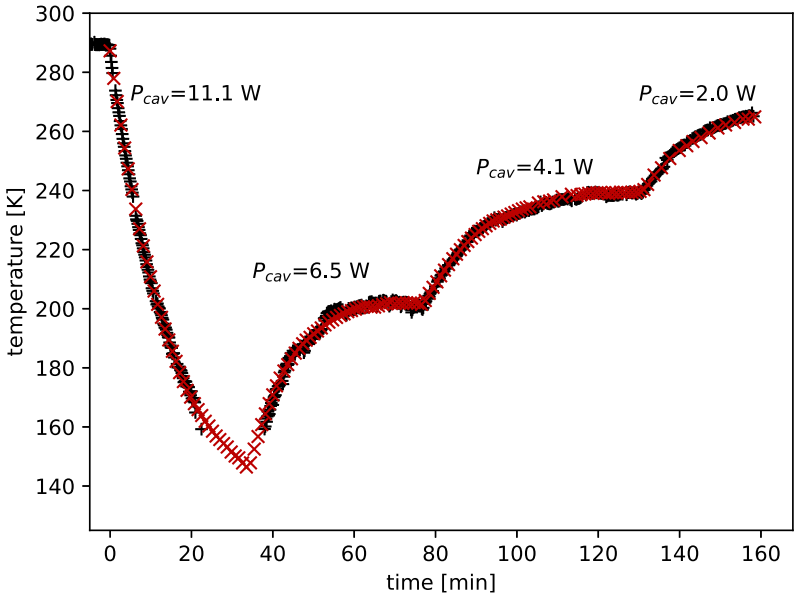

Fig. 2. DLT calibration experiment: at time $t>0$ the cooling laser is switched on. The crystal temperature is measured with the camera (corrected temperature T_c, black +) and spectra are continuously monitored. Four different in-cavity laser powers P_{cav} are used successively.

4. Results and discussion

The experimental run reaching the minimum attainable temperature (MAT) is shown on Fig. 3. At time $t = 0$ the cooling laser is switched on (in cavity power $P_{cav} = 11.1(4)$ W) and the crystal temperature is monitored by both the thermal camera and the DLT. After 40 min, the crystal reaches the minimal attainable temperature $T_{MAT} = 125(5)$ K, with a temperature decrease of $\Delta T = 163$ K. The conditions of operation remain stable for about 1 h: the crystal temperature increase is less than 2 K and can be explained by a small increase of the clamshell temperature. At time $t = 95$ min, the laser is switched off. Hence only the camera provides an information about the return of the crystal to thermal equilibrium with the clamshell (equilibrium temperature $T_0 = 288$ K). During this period, the crystal temperature is only subjected to heat transfer by conduction, convection and radiation:

$$\rho V_c c_v(T) \frac{dT}{dt} = P_1 \frac{T - T_0}{T_{MAT} - T_0} + P_R \frac{T^4 - T_0^4}{T_{MAT}^4 - T_0^4}, \tag{3}$$

where $\rho = 3.99\,\mathrm{g \cdot cm^{-3}}$ is the density of YLF and V_c is the crystal volume. $c_v(T)$ is the temperature-dependent heat capacity of doped YLF [15]. P_1 is the sum of the conductive and convective heat load and P_r is the radiative heat load at the MAT respectively. The dashed blue line on Fig. 3 is the solution to Eq. (3) with $P_1 = 12.7$ mW and $P_R = 8.3$ mW which are best fitted to the experimental data. In order to cross-check and validate the DLT extrapolation method, we estimated the crystal's final temperature attained just before the laser was switched off. This can be done by solving the thermal model for times anterior to the first thermal camera reading around 100 min, knowing exactly the time when the laser was switched off. We find a crystal temperature of T = 118(5) K, in agreement with the final DLT predicted temperature considering the estimated errors for both measurements.

Optics EXPRESS

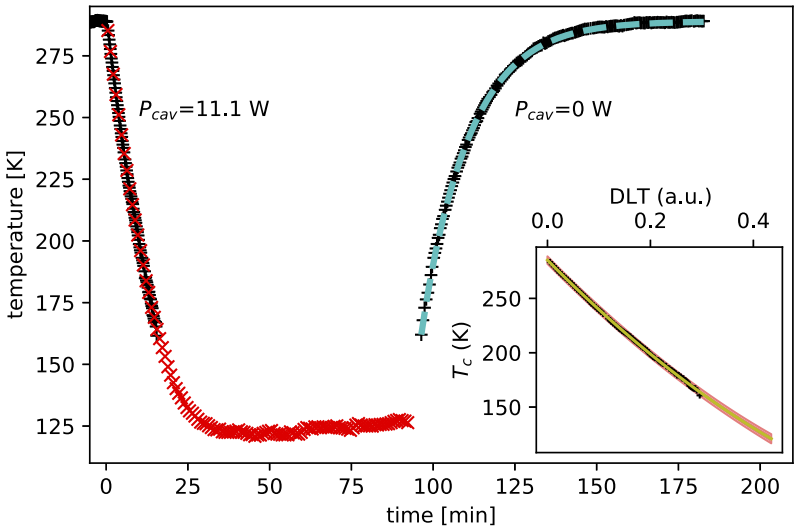

Fig. 3. Crystal cooling run for an in-cavity laser power of 11.1 W, starting at time $t = 0$. The camera temperatures (black +) and the spectroscopic temperature (red ×) are recorded. At time $t = 95$, the laser is switched off. The dashed blue line corresponds to a best fit of the data by the solution of Eq. (3) with $P_1 = 12.7$ mW and $P_R = 8.3$ mW. The inset shows the calibration of DLT signal. The yellow curve is the polynomial fit and the red area corresponds to the 95 % prediction band.

In our experiment we limit the laser power to ~ 11 W for two reasons: the first is related to the matching between the reached temperature and the values needed in many space cryogenic setups; the second is that increasing the pump power the temperature doesn't decrease anymore, probably because of the imperfect alignment leading to extra heating source.

The above mentioned heat load can be compared to the cooling power:

$$P_{cool} = \eta_c(\lambda, T) P_{abs} = \eta_e \frac{\alpha(\lambda, T)}{\alpha(\lambda, T) + \alpha_b} \left(\frac{\lambda}{\lambda_f(T)} - 1 \right), \tag{4}$$

where P_{abs} is the laser power absorbed in the crystal and $\eta_c(\lambda, T)$ is the cooling efficiency. Absorption and fluorescence spectra measured as a function of temperature T allow to determine the YLF absorption coefficient $\alpha(\lambda, T)$ and the mean fluorescence wavelength $\lambda_f(T)$ [16]. Finally η_e and $\alpha_b(T)$ the external quantum efficiency and the background absorption coefficient by impurities in the crystal. Figure 4(a) shows the cooling efficiency of the sample as a function of pump wavelength, measured at room temperature. The experimental data are fitted with the standard model described in Eq. (4), giving for the value of the two parameters $\eta_e = 0.987$ (3) and $\alpha_b = 2.6(3) \cdot 10^{-4}$ cm^{-1}.

Figure 4(b) presents the cooling efficiency $\eta_c(\lambda, T)$ using Eq. (4). On this graph the point of operation at the MAT is represented by a black cross and the dash-dotted line presents the thermal equilibrium condition $\eta_c P_{cav} = P_1 + P_R$. We note that our experimental results cannot be explained by keeping constant values for η_e and α_b. Using the fitted values of Fig. 4(a) yields to a minimum attainable temperature of 135 K at zero cooling power and 175 K at $P_1 + P_R$. The need to have a temperature varying background absorption to explain properly the cooling performance at both room and cryogenic temperatures has already been evidenced in Ref. [10]. It was proposed that the dominant contribution to background absorption takes place from thermally activated excited states $\alpha_b \propto \exp -T_b/T$, with $T_b = 387.6$ K. Using this modified model in Eq. (4)

Optics EXPRESS

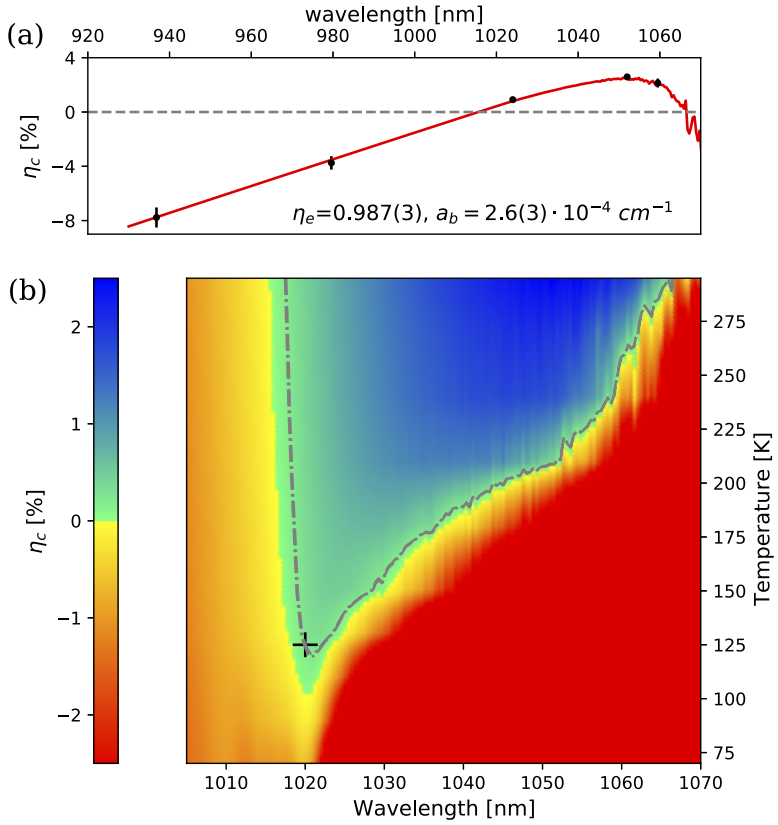

Fig. 4. (a) Cooling efficiency trend of the sample at room temperature. Experimental data (black +) are fitted with the model of Eq. (4). (b) Cooling efficiency $\eta_c(\lambda, T)$ with a modified model of Eq. (4), where η_e and α_b depend on T. The black cross corresponds to the MAT point of operation. The dash-dotted contour line corresponds to the thermal equilibrium condition $\eta_c P_{cav} = P_1 + P_R$.

yields to a minimum temperature at zero cooling power lower than T_{MAT} but is not completely satisfactory as it predicts an equilibrium temperature of 150 K at $P_{cool} = P_1 + P_R$.

To fully explain our results we have evaluated the external quantum efficiency by numerical simulation using a ray tracing software [17] that accounts for the temperature dependent fluorescence and absorption spectra of Yb:YLF [18]. Neglecting the birefringence of the crystal and averaging the spectra for the two polarization (unpolarized approximation), we observe that η_e systematically increases by $\sim 0.25\%$ as the crystal is cooled from 300 to 100 K. This increase is due to the decrease of the absorption by both Yb and impurities, leading to a higher escape probability for a fluorescence photon. We note that its magnitude is of the order of the fitting error for η_e in Fig. 4(a). Simulations show that the variation of η_e can be assumed to be linear in the temperature range of interest. It is hence characterized by its value at 100 K, η_e(100K). With the modified model for both η_e and α_b we have explored the parameter space for T_b and η_e(100 K) that are in agreement with the thermal equilibrium at T_{MAT}. Figure 4(b) present the results for T_b = 200 K and η_e(100 K) = 0.99. Our model gives very satisfactory results for T_b in the 150 – 250 K range, with η_e(100 K) varying concurrently from 0.9903 to 0.9895. For this range of parameters the minimum temperature at zero cooling power varies between 108 and 95 K, a value which stays in good agreement with previous observations on Yb:YLF crystals.

Optics EXPRESS

5. Conclusion

We have successfully implemented a fiber-coupled lasercooler prototype whose cold head performances in terms of conductive and radiation losses matches the state of the art. The temperature reached matches with the typical value needed in many space cryogenics setups. This paves the way towards obtaining lower MAT with more efficient crystals [8]. The next step is to implement in the experiment the thermal link between the cooling head and the scientific load [4,19].

Funding. Association Nationale de la Recherche et de la Technologie (CIFRE 2018-0065).

Acknowledgements. Rémi Vicente was supported by a PhD grant from French National Association for Research and Technology (ANRT) under CIFRE contract number 2018-0065. The featured developments were funded by Air Liquide Advanced Technologies and Institut Néel, CNRS. The University of Pisa and Mega Materials provided support in lending cooling grade crystals for research purposes and technical expertise regarding the characterization of those crystals. The authors would like to acknowledge I. Grassini for her competence and care in preparing the crystal sample; and the technological platforms at Institut Néel which helped designing and building the experiments.

Disclosures. ADL and MT: Mega Materials (I,S).

Data availability. Data underlying the results presented in this paper are not publicly available at this time but may be obtained from the authors upon reasonable request.

References

1. R. I. Epstein, M. I. Buchwald, B. C. Edwards, T. R. Gosnell, and C. E. Mungan, "Observation of laser-induced fluorescent cooling of a solid," Nature **377**(6549), 500–503 (1995).
2. J. Thiede, J. Distel, S. R. Greenfield, and R. I. Epstein, "Cooling to 208K by optical refrigeration," Appl. Phys. Lett. **86**(15), 154107 (2005).
3. D. V. Seletskiy, S. D. Melgaard, A. D. Lieto, M. Tonelli, and M. Sheik-Bahae, "Laser cooling of a semiconductor load to 165 K," Opt. Express **18**(17), 18061–18066 (2010).
4. M. P. Hehlen, J. Meng, A. R. Albrecht, E. R. Lee, A. Gragossian, S. P. Love, C. E. Hamilton, R. I. Epstein, and M. Sheik-Bahae, "First demonstration of an all-solid-state optical cryocooler," Light: Sci. Appl. **7**(1), 15 (2018).
5. S. R. Bowman, "Lasers without internal heat generation," IEEE J. Quantum Electron. **35**(1), 115–122 (1999).
6. S. R. Bowman, S. P. O'Connor, S. Biswal, N. J. Condon, and A. Rosenberg, "Minimizing heat generation in solid-state lasers," IEEE J. Quantum Electron. **46**(7), 1076–1085 (2010).
7. R. Vicente, G. Nogues, J.-M. Niot, T. Wiertz, P. Contini, and A. Gardelein, "Impacts of laser cooling for low earth orbit observation satellites: An analysis in terms of size, weight and power," Cryogenics **105**, 103000 (2020).
8. G. Cittadino, E. Damiano, A. D. Lieto, and M. Tonelli, "First demonstration of optical refrigeration efficiency greater than 4% at room temperature," Opt. Express **28**(10), 14476–14489 (2020).
9. S. D. Melgaard, A. R. Albrecht, M. P. Hehlen, and M. Sheik-Bahae, "Solid-state optical refrigeration to sub-100 Kelvin regime," Sci. Rep. **6**(1), 20380 (2016).
10. A. Volpi, J. Meng, A. Gragossian, A. R. Albrecht, S. Rostami, A. D. Lieto, R. I. Epstein, M. Tonelli, M. P. Hehlen, and M. Sheik-Bahae, "Optical refrigeration: the role of parasitic absorption at cryogenic temperatures," Opt. Express **27**(21), 29710–29718 (2019).
11. J. B. McManus, P. L. Kebabian, and M. S. Zahniser, "Astigmatic mirror multipass absorption cells for long-path-length spectroscopy," Appl. Opt. **34**(18), 3336–3348 (1995).
12. A. Gragossian, J. Meng, M. Ghasemkhani, A. R. Albrecht, and M. Sheik-Bahae, "Astigmatic Herriott cell for optical refrigeration," Opt. Eng. **56**(1), 011110 (2016).
13. D. V. Seletskiy, S. D. Melgaard, S. Bigotta, A. D. Lieto, M. Tonelli, and M. Sheik-Bahae, "Laser cooling of solids to cryogenic temperatures," Nat. Photonics **4**(3), 161–164 (2010).
14. Q. Mermillod, J. Cazals, A. Glière, M. Dupoy, N. Aubert, and S. Chabardès, "Laser cooling of solids: towards biomedical applications," Proc. SPIE **10936**, 1 (2019).
15. R. L. Aggarwal, D. J. Ripin, J. R. Ochoa, and T. Y. Fan, "Measurement of thermo-optic properties of $Y_3Al_5O_{12}$, $Lu_3Al_5O_{12}$, $YAlO_3$, $LiYF_4$, $LiLuF_4$, BaY_2F_8, $KGd(WO_4)_2$, and $KY(WO_4)_2$ laser crystals in the 80-300K temperature range," J. Appl. Phys. **98**(10), 103514 (2005).
16. D. V. Seletskiy, M. P. Hehlen, R. I. Epstein, and M. Sheik-Bahae, "Cryogenic optical refrigeration," Adv. Opt. Photonics **4**(1), 78–107 (2012).
17. M. J. Hayford and S. R. David, "Characterization of illumination systems using LightTools," Proc. SPIE **3130**, 209–220 (1997).
18. S. Püschel, S. Kalusniak, C. Kränkel, and H. Tanaka, "Temperature-dependent radiative lifetime of Yb:YLF: refined cross sections and potential for laser cooling," Opt. Express **29**(7), 11106–11120 (2021).
19. S. D. Melgaard, J. Trevino, D. V. Seletskiy, and M. Sheik-Bahae, "Novel photon blockade schemes for thermal link applications," Proc. SPIE **8275**, 75–79 (2012).